The use of CFD in the evaluation of UV treatment systems

N. G. Wright and D. M. Hargreaves

ABSTRACT

UV disinfection is now widely used for the treatment of water for consumption and wastewater in many countries. It offers advantages over other techniques in specific circumstances. Analysis of these systems has been carried out using a three-dimensional Computational Fluid Dynamics (CFD) procedure. This allows for efficient testing of prototypes. Sensitivity tests are shown for grid size, discretisation and turbulence model.

Four different configurations of the apparatus are evaluated in terms of maximum dosage, flow patterns, particle tracks and transient dosage. This leads to conclusions about the most efficient design and shows that significant improvements can be achieved with minor changes to the design. Further conclusions are drawn about the CFD procedure itself. This work opens up the possibility of an internet-based design tool for small- and medium-sized enterprises.

Key words | water treatment, computational fluid dynamics, ultraviolet treatment

N. G. Wright (corresponding author)
School of Civil Engineering,
University of Nottingham,
Nottingham NG7 2RD,
UK
Telephone +44 115 951 3899;
Fax +44 115 951 3898;
E-mail: *nigel.wright@nottingham.ac.uk*

D. M. Hargreaves
School of Chemical,
Environmental and Mining Engineering,
University of Nottingham,
Nottingham NG7 2RD,
UK

INTRODUCTION

The use of 3D Computational Fluid Dynamics (CFD) analysis is becoming widespread in many branches of engineering (Versteeg & Malalaskera 1996). Use is made of software originally developed in mechanical and process engineering for applications such as nuclear engineering and aircraft design. Increasingly, this technique is being introduced into civil and environmental engineering. It offers the advantage of rapid design and prototyping and the opportunity to test failure modes that would be undesirable, or even impossible, to reproduce physically. The analysis can also provide more detailed results than physical models, which are restricted by the number of measuring points, scaling effects or the accessibility of the flow. Computer methods for solving the shallow water equations have been widely used in river, estuarine and coastal engineering (Falconer 1992). This paper focuses on the more generic class of 3D CFD software that solves the full three-dimensional Navier–Stokes equations. As mentioned above, CFD software is designed for general application and the authors have experience of using this software in a number of areas such as wind effects on buildings (Wright & Easom 1999), natural ventilation (Straw 2000), pollutant dispersion (Richards *et al*. 2000) and meandering river channels (Morvan *et al*. 2000). Validation of CFD and the software used here is given in these references and elsewhere (AEA Technology 1999*a*, *b*).

The application of CFD in new areas is becoming increasingly feasible and accessible due to recent advances in CFD technology and computer hardware. The availability of unstructured grids assists the application to complex geometry and decreases the engineer's time in setting up a particular problem. The latter can be a major overhead. The increased sophistication of mathematical models for phenomena such as free surfaces, multiphase flow and chemical reaction allows for application to a wider range of situations. Advances in computer hardware mean that many CFD applications can be run on a desktop or portable PC. This move from specialist UNIX workstation to a relatively cheap, commodity product gives a reduction in purchase cost and cost of ownership, which in turn greatly widens the potential user base. As with any new technology care must be taken to use CFD correctly and appropriately and a number of such issues will be addressed in this paper.

This paper demonstrates the potential of CFD through its application to the UV treatment of water. UV treatment (Cairns & MacDonald 1995) is a photochemical disinfection process that is used to treat both water supply and wastewater. It can be particularly useful for treating grey wastewater for re-use. The process involves passing water in the vicinity of a low-pressure mercury lamp which emits short wave radiation at a wavelength near to 254 nm. This radiation kills micro-organisms by altering their DNA, which prevents them from dividing and reproducing. UV treatment has the advantage of leaving no residue in the water and consequently not posing an environmental risk from leakage or spillage. However, there are the associated costs of pumping and running the UV tubes which must be minimised by careful design.

The use of CFD in the design of UV treatment units offers a significant speed-up in the design process, which seeks an optimal solution by balancing the various design drivers. In short, adequate disinfection is required for a minimum energy cost. This will come about through minimising short-circuiting and head losses in the UV tubes as the pumping requirements consume energy. In addition to use in the design process, CFD can be used to investigate problems in existing installations that are not performing satisfactorily.

METHODS

The work presented here has been carried out with a commercial software package called CFX5 (AEA Technology 1999*a*). This was possible as all the necessary simulation features were available within CFX5 and therefore there was no need to develop a bespoke code. Additional advantages are the comprehensive validation and the ease of transfer of the results to end-users.

For this work an unstructured mesh consisting of tetrahedral elements was used. Although the geometry of the UV systems considered here is only constructed from cylindrical shapes, the joining of these can present complications when generating a mesh and poor grid structure if a structured grid approach is adopted. Once the grid has been created, the governing equations of conservation of mass and momentum are solved in each cell. This results in a set of simultaneous algebraic equations for all elements, which is solved using an algebraic multigrid technique (Raw 1994).

CFX5 uses an unstructured tetrahedral mesh and solves the equations through a finite volume method based on values stored at cell vertices. Both first-order and second-order spatial discretisation can be used to calculate the fluxes in the discretised equations. Spurious pressure oscillations are prevented through the use of a fourth-order pressure smoothing procedure (Rhie & Chow 1982). The resulting algebraic equations are solved in a coupled fashion as opposed to the predominantly used segregated approach that solves each velocity and pressure separately in sequence. This delivers a faster and more robust procedure at the expense of memory usage. In addition, an algebraic multigrid method is used in conjunction with an incomplete LU decomposition (ILU) smoother to solve the equations efficiently, even on large meshes. In the authors' experience meshes of over 3 million cells are not impractical. For more detailed information readers are referred to other publications (Hutchinson & Raithby 1986; Schneider & Raw 1987; Raw 1994; AEA Technology 1999*a*).

Turbulence occurs in the fluid flows considered here and the standard k–ε model (Launder & Spalding 1974) is used to represent the effects of this on the mean velocities. This models the effects of turbulence on the mean velocities by means of a turbulent eddy viscosity which is analogous to molecular viscosity. The value of the eddy viscosity is set by the following equation based on values of turbulent kinetic energy, k, and turbulent energy dissipation, ε:

$$\mu_t = \rho C_\mu k^2/\mu$$

where C_μ is a constant, ρ is the density and k and ε are calculated using additional equations representing their production, destruction and transport. Further details can be found in the literature (Launder & Spalding 1974). The standard k–ε model is known to give poor results in the case of swirling pipe flow. Although the geometry here differs through the inclusion of a central obstruction it was considered appropriate to evaluate other turbulence

models to see if a better treatment of turbulence gave significantly different results. The additional models evaluated are the Re-normalised Group (RNG) k–ε model (Yakhot *et al*. 1992) and the Differential Reynolds Stress Model (Launder *et al*. 1975). The former includes changes that have improved results in other fields and the latter contains an anisotropic treatment of turbulence, as opposed to the isotropic eddy viscosity concept used in the k–ε model. The results of these comparisons will be shown later.

As the fluid flow approaches a wall, rapid changes in velocity occur as the fluid is brought to rest at the wall. This results in high velocity gradients and shear stresses. To accurately model these would require very fine meshes in the boundary region. In order to avoid this a wall function approach is used (Versteeg & Malalaskera 1996). This replaces the usual discretisation with a function based on an analysis of near-wall flow in a generic case.

In general, CFD analyses provide predictions of velocities and pressure at steady state. This gives information about head loss through the system and flow patterns. It is increasingly acknowledged that this information is not sufficient in itself to give information to designers who have little understanding of fluid analysis techniques and CFD outputs in particular. UV treatment is no exception to this. Meaningful measures of the performance of the disinfection system require further analysis in terms of the design drivers. Provision of these analysis tools provides a hydroinformatics system that can readily assist in design. This design methodology can be configured as an internet-based system where a designer uses an internet browser application to design a configuration and in turn this application transmits the design parameters to an analysis site. This site carries out the analysis and returns the results for display on the designer's internet station (van Doormaal 1999). The internet browser application can be set up with a limited subset of options containing only those of relevance to the user's applications area. Setting up the design tools is addressed later, but the possible internet solution is not presented here.

Base case and other configurations

A number of different geometries were built around the basic design shown in Figure 1 (showing configuration 1—the 'base case'). The actual dimensions of the model were taken to be representative of a commercial design and are given below:

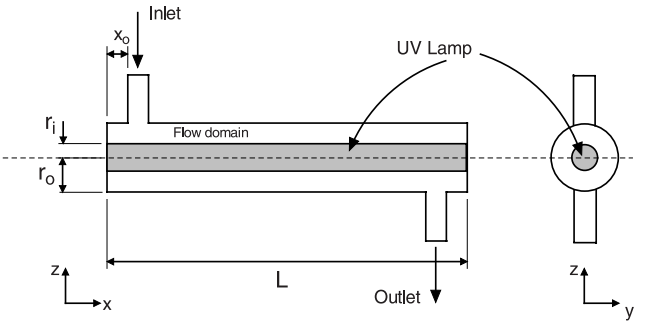

Figure 1 | A schematic of the UV tube in configuration No. 1.

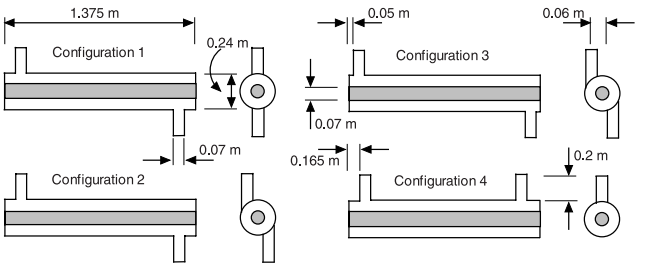

Figure 2 | The different configurations of UV tube used in the study.

Length, L	1.375 m
Inner radius, r_i	0.035 m
Outer radius, r_o	0.120 m
Inlet/outlet offset from ends, x_o	0.165 m
Inlet/outlet radius	0.035 m

Figure 2 shows the base case and three variants that were tested in this work. Configuration 2 differs from the base case by having the inlet/outlet pipes offset laterally from the centre of the pipe. Configuration 3 differs from configuration 2 by having the distance x_o of the inlet/outlet pipe from the end reduced to 0.05 m. Configuration 4 has the inlet/outlet pipes on the same side. These variations represent only a small number of possible changes, but do reveal how CFD can be used to efficiently evaluate design changes. A normal speed of 0.5 m s^{-1} was specified at the inlet and a relative pressure of 0.0 Pa was

set at the outlet. All other surfaces are specified as smooth, no-slip surfaces.

UV DOSE AND PARTICLE TRACKING

The steady state solution for the continuity and momentum equations will give a value for the head loss across the system. This is an important parameter, but other techniques are still necessary to give insight into the suitability of different designs. In this work two techniques have been used: UV doses (steady and transient) and particle tracking.

UV dose

Cairns & MacDonald (1995) define the dose of UV delivered to a disinfecting device as the product of the average light intensity I_{ave} (typical units: μW cm^{-2}) within the device and the average retention or residence time, t_R(s) of the water passing through the device. For example, faecal coliforms require about 3.4 mW s cm^{-2} of additional UV dose to inactivate an order of magnitude of microbes. To achieve 99% inactivation (i.e. two orders of magnitude) would therefore require a 6.8 mW s cm^{-2} dose of UV.

In order to obtain residence times from CFD models a user scalar is used to represent residence time. This variable has a source term of 1.0 s s^{-1} throughout the flow domain so that fluid that remains in the system for 1 second has a 1 second increase in residence time. A steady state solution is then obtained based on a previously calculated velocity and pressure field and the calculated 'concentration' of this scalar at each point is equal to the residence time of fluid passing through that point.

In the UV disinfection device this method can be adapted to predict the effect of disinfection. The UV lamp represents a line source with maximum light intensity I_{max} at its surface at a radius r_i. It can be seen from Figure 3 that the area of a infinitesimal patch on the UV lamp is $r_i\Delta\theta\Delta x$, where $\Delta\theta$ is some small angle and Δx is an infinitesimal length of the UV lamp (aligned with the x axis). As the radius increases to r, the dimension of the patch increases only in the circumferential direction and thus the area increases to $r\Delta\theta\Delta x$. In this work it is assumed that the energy from the lamp is not attenuated by the water and so is constant and it follows that

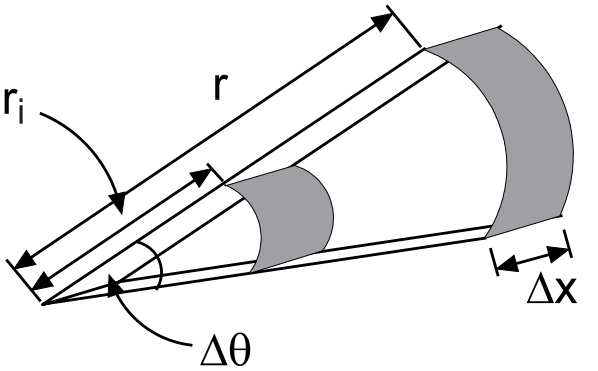

Figure 3 | Schematic of the increase in area over which the constant power from the UV lamp is dissipated.

$$I_{max} r_i \Delta\theta \Delta x = I(r) r \Delta\theta \Delta x$$

from which $I(r) = I_{max}(r_i/r)$. Combining this relationship with the residence time and using this as the source of the scalar means that the 'concentration' of the scalar will be equal to the dose of UV that has been received by the fluid at any point in the domain. Since the aim of this investigation is to compare only the relative efficiencies of different designs, I_{max} is set to 1 W m^{-2} (or 0.1 mW cm^{-2}) throughout. The dose is limited by r_o and so no dose is given to the side arms.

Particle tracks

Particle tracks allow the design engineer to easily visualise the fluid flow. The tracks are calculated through Lagrangian tracking. The trajectory of an individual particle is calculated from its initial position by solving equations at each time step based on the velocity at its current point:

$$\frac{d\boldsymbol{R}}{dt} = \boldsymbol{u}(\boldsymbol{R})$$

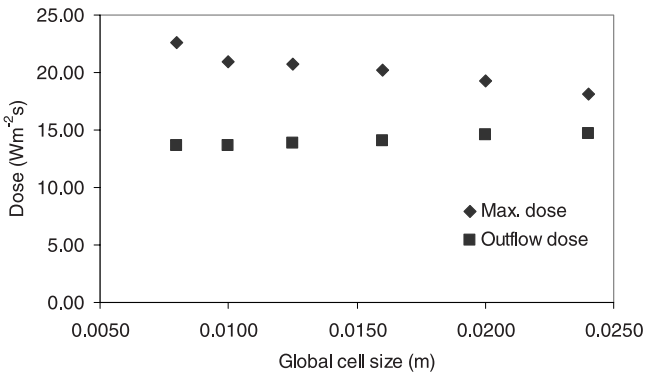

Figure 4 | Plot of maximum dose in the domain and mean outflow dose against the global cell size in the domain.

where $\boldsymbol{R}$ is the spatial position of the particle and $\boldsymbol{u}$ is the fluid velocity. If a sufficiently large number of particles are released at the inlet an accurate picture of the flow can be built up. In addition, the dosage of UV received by these imaginary bacteria can be calculated and the total dosage received can be read from the value as the particle leaves the domain.

RESULTS AND DISCUSSION

In any CFD analysis it is essential to test the sensitivity of the results to various aspects of the CFD algorithm. Only once this has been done can it be certain that results are realistic rather than the product of a numerical artefact.

Sensitivity to mesh density

Using the mean value of the dose in the outflow and the maximum dose in the domain as a guide, a grid sensitivity study was conducted. There was no localised refinement of the grid used—a single global element size was prescribed. Results using configuration 3 (Figure 4) showed that there was a significant difference in both the mean outflow and domain maximum dosages between a global mesh size of 0.024 m and 0.020 m. However, a further reduction to 0.016 m showed no significant change and so this mesh was used throughout the remainder of the tests. This mesh size resulted in approximately 135,000 cells. Further reductions to mesh sizes of 0.0125, 0.010 and 0.008 showed little change. Sensitivity tests were also conducted for the other configurations and revealed similar trends.

Sensitivity to discretisation

Again for configuration 3, the effect of using the different differencing schemes in CFX5 was investigated. In CFX5, a 'blend' factor is available to the user to control the level of robustness of the solution against the accuracy of the solution. The blend factor ranges from 0.0 for a first-order discretisation that is a robust and reliable solution to 1.0 for a second-order solution that is more accurate. Figure 5 shows the effect of moving from the default blend factor of 0.0 (used throughout these tests) to values of 0.5 and 0.75. Both the latter runs were restarts from the robust solution using a blend factor of 0.0. The plots show the variation of the u and w components of the flow, the turbulent kinetic energy and the dose along a profile parallel to the y axis at 0.5 m from the inlet. The increases in dose are particularly large for the more accurate schemes. Because of these significant differences, it was decided to conduct the remainder of the numerical tests using the blend factor of 0.75 to achieve high accuracy. Restarts from the more robust case were used throughout.

Sensitivity to choice of turbulence model

The sensitivity of the flow and turbulence fields to the particular turbulence model was also studied for configuration 3 with the 0.75 blend factor. In addition to the standard k–ε model, the RNG k–ε and Differential Reynolds Stress models were used. It is normal practice to use the k–ε model, as the Reynolds Stress Model usually requires much longer computer runs. Figure 6 shows results for the different models at the same traverse as was used in the last section. In all three cases, the velocity and dosage results varied very slightly, as shown in Figure 6. There is a large variation in values of turbulent kinetic energy between the k–ε models and the Reynolds Stress

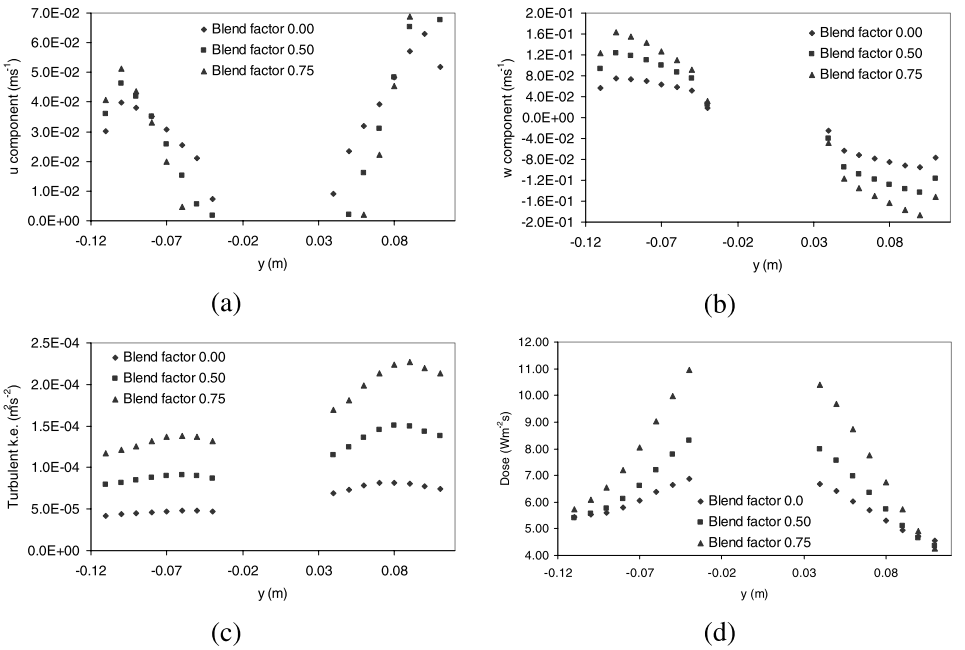

Figure 5 | Plots showing sensitivity of the model of configuration 3 to changes in blend factor for (a) *u* component of flow, (b) *w* component of flow, (c) turbulent kinetic energy and (d) dose.

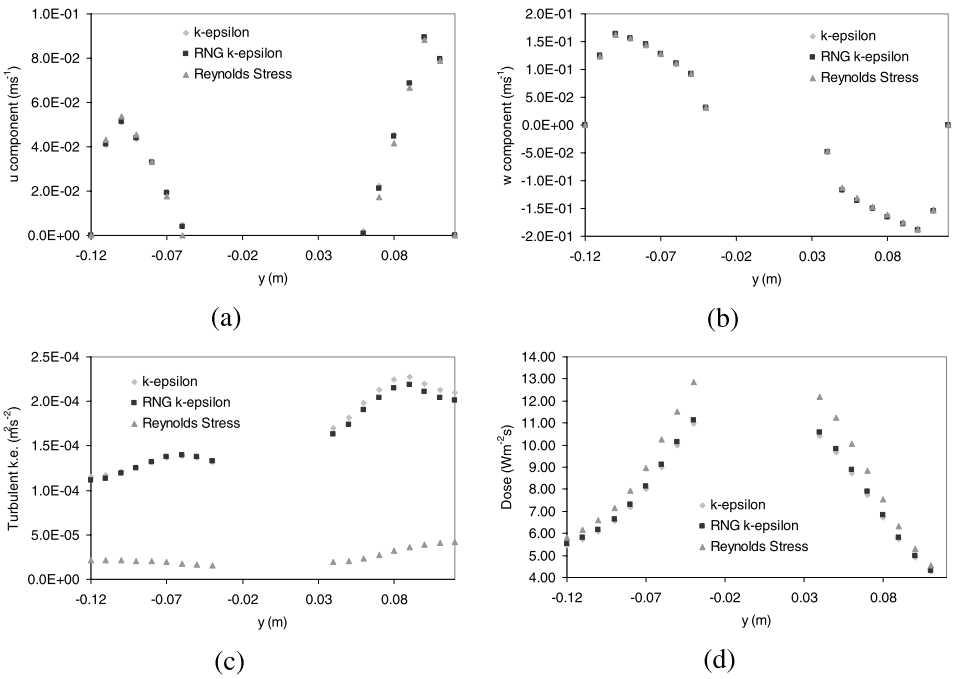

Figure 6 | Plots showing sensitivity of the model of configuration 3 to changes in turbulence model for (a) *u* component of flow, (b) *w* component of flow, (c) turbulent kinetic energy and (d) dose.

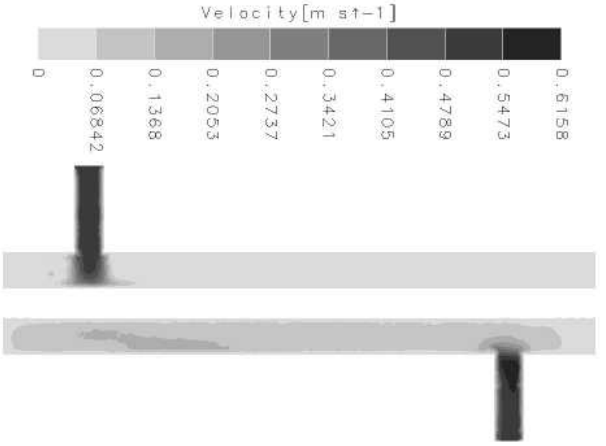

Figure 7 | Speed contours on a centrally located *xz* plane for configuration 1.

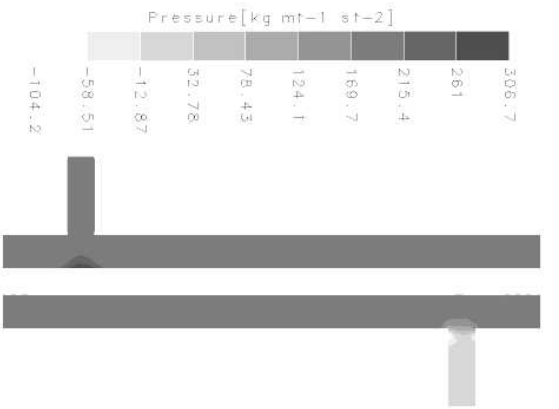

Figure 8 | Pressure contours on a centrally located *xz* plane for configuration 1.

Model. This is not unexpected as the latter solves for each component of the Reynolds stresses rather than the total kinetic energy. The difference in k has a small effect on dosage due to turbulent diffusion and little effect on the velocity so the k–ε model was deemed sufficiently accurate for the comparative study undertaken here in view of the increased computational requirements of the Reynolds Stress Model. On average, the latter required computer runs that were a factor of 3–4 larger than k–ε.

Flow field

For the base case, a pseudo-timestep size of 5 s was used to achieve convergence in the steady state. Figure 7 shows speed and Figure 8 pressure contours on a plane which cuts through the body of the UV tube and the feeder and outflow pipes. As expected, the flow velocity is significant in the side arms and is low in the body of the tube, which has a much greater cross-sectional area. The greatest pressures in this case are seen at the point on the UV lamp where the inlet flow impinges.

In configurations 2 and 3, there is a significant swirl in the flow around the central UV lamp. Figures 9–12 show particle tracks for configurations 1–4. The effect of offsetting the side tubes can be seen in the generation of swirl—a phenomenon which is absent when the side arms are located on the axis of the UV tube.

Pressure losses

An important issue relating to the design of such devices is to minimise the head loss in the device, thus reducing the pumping requirement. Table 1 shows the pressure drop from inlet to outlet for each of the four configurations. The largest pressure drops correspond to the configurations with the largest swirl component in the flow. The increased pressure drop is due to the longer effective flow path through these configurations (2 and 3).

Dosage

Steady state conditions

Table 1 also shows the maximum dosage seen in the flow domain for the different configurations. Configuration 4 has the largest maximum by some margin, which indicates inefficiency in its operation. This is emphasised further by Figure 13 which shows the dose on a central plane for each configuration. The same scale from 0 to 60 W m^{-2} s is used in each plot to highlight the differences. Both configurations 2 and 3, where swirl is present, provide smoother variations in the dose, with 3 showing the smoothest pattern of all since the inlet and outlet pipes are situated close to the ends of the device. Also, configuration 3 shows higher doses closer to the UV tube at a fixed distance along the tube, which demonstrates the effect of

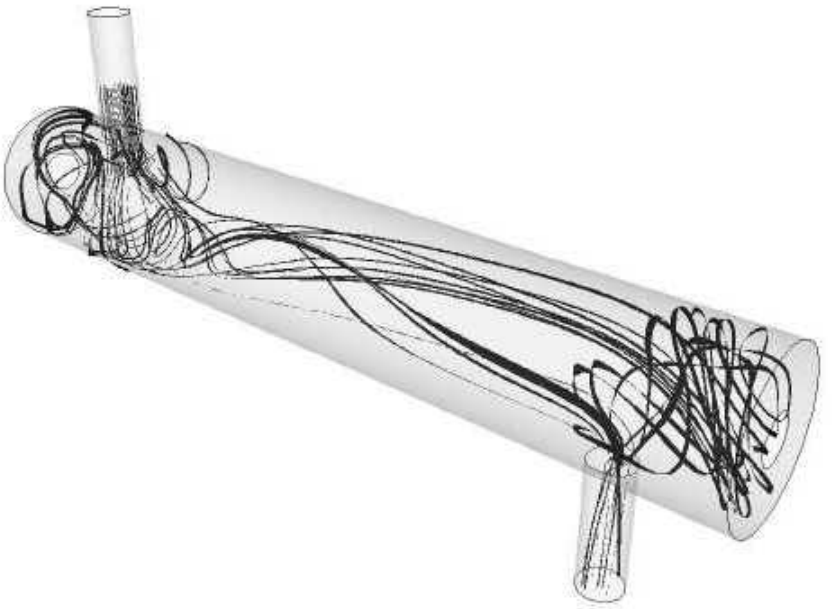

Figure 9 | Particle tracks coloured by dose for configuration 1.

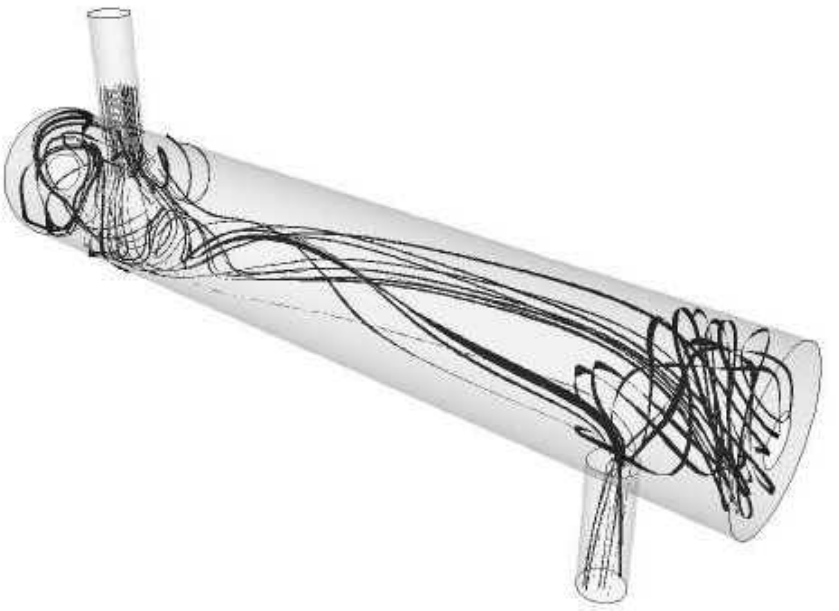

Figure 10 | Particle tracks coloured by dose for configuration 2.

the source term which varies as $1/r$. The increase in efficiency through the reduction of maximum dosage (i.e. dosage significantly over the mean) is offset by an increase in head loss. However, it can be seen from Table 1 that a 5% increase in head loss has given a 20% decrease in maximum dosage, which should give an overall gain.

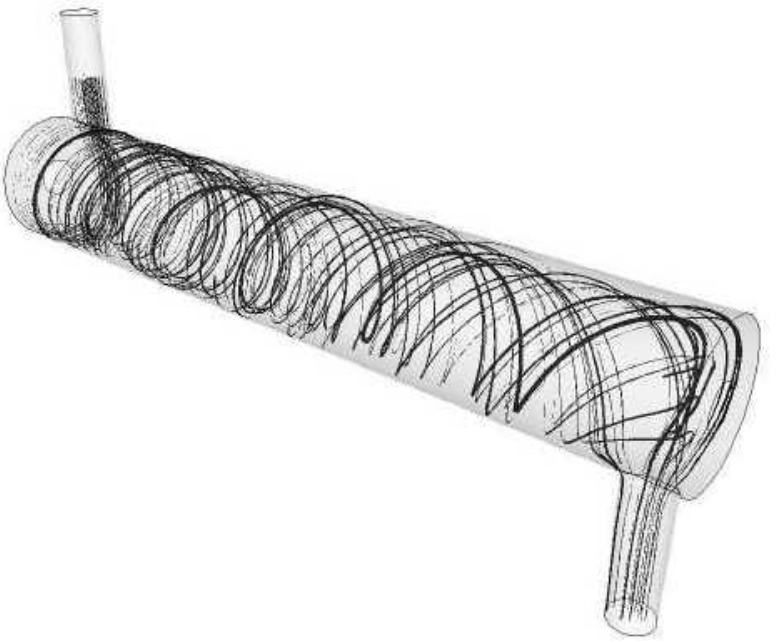

Figure 11 | Particle tracks coloured by dose for configuration 3.

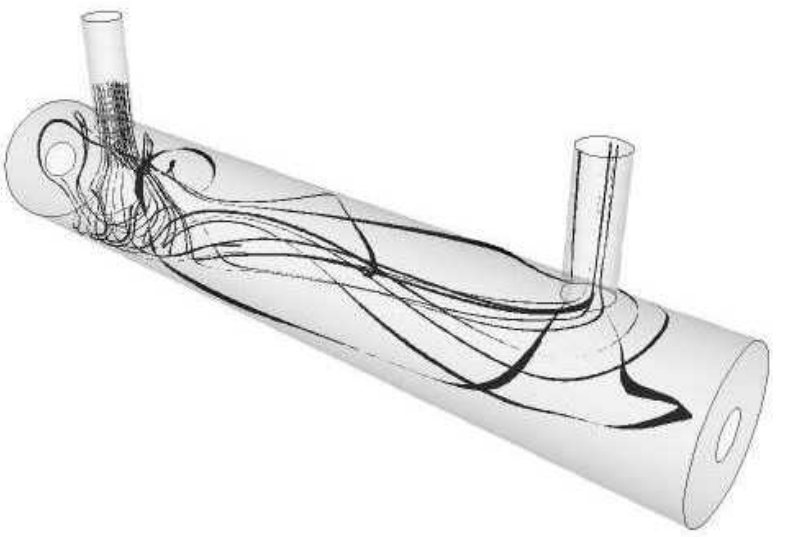

Figure 12 | Particle tracks coloured by dose for configuration 4.

Transient conditions

Several solutions were obtained for transient situations. While not indicative of the operation of UV disinfection devices, which in practice are run continuously, such computational experiments provide important insights into their operation. They also replicate the experimental

Table 1 | Maximum dose seen in the device and pressure drop across the device for the difference configurations

	Max. dose (W m^{-2} s)	Pressure drop (Pa)
Configuration 1	30.6	190.2
Configuration 2	24.6	203.6
Configuration 3	20.2	201.9
Configuration 4	57.6	182.3

procedure of introducing a plug of substance and measuring the outlet concentration.

These runs were restarts from successful steady state runs where the source of the dose had not been included. After 2 s of the transient run, the UV tube was effectively switched on by introducing a source of the dose for the next 5 s. After that the dosing was switched off and the solution allowed to run up to a total time of 60 s.

Under these conditions (which simulate a burst of UV radiation to the water), it is possible to plot the outflow of dose against time (Figure 14(a)). All configurations exhibit a similar maximum, which corresponds to the local dose near the outflow pipe breaking through to the outlet. It is the variation after the UV is turned off which is revealing. The trace for configuration 3 shows a second peak which is due to the remainder of the dose exiting the device. None of the other configurations demonstrate this peak because the rate of dosage clearance is much slower in these cases. This effect is further confirmed in Figure 14(b) which shows the cumulative dose lost at the outlet. Configuration 3 reaches a plateau earlier than the others, demonstrating the more efficient movement of dosed water through the device. It is possible to compare the final total of dose from the outlet with the theoretical dose received by the water during the burst of radiation. The theoretical total dose is given by

$$D_{\text{total}} = \int_0^L \mathrm{d}x \int_0^T \mathrm{d}t \int_{r_i}^{r_o} 2\pi I_{\max} \left(\frac{r_i}{r}\right) r\,\mathrm{d}r = 2\pi LTr_i(r_o - r_i) \ (\mathrm{m}^3\,\mathrm{s}) \quad (2)$$

where T (s) is the duration of the burst of UV radiation. Evaluation of Equation (2) for this geometry and flow rate gives a total of 1.28×10^{-1} W m^{-2} s, which compares exactly with the cumulative total for configuration 3. All the other configurations would tend to this value, given longer run times.

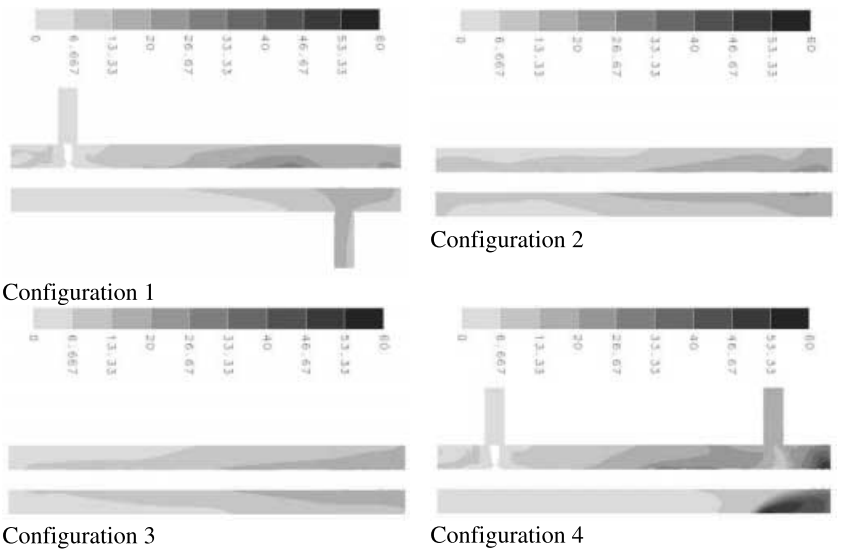

Figure 13 | Plots of dose (W m^{-2} s) for the four configurations on a centrally located plane.

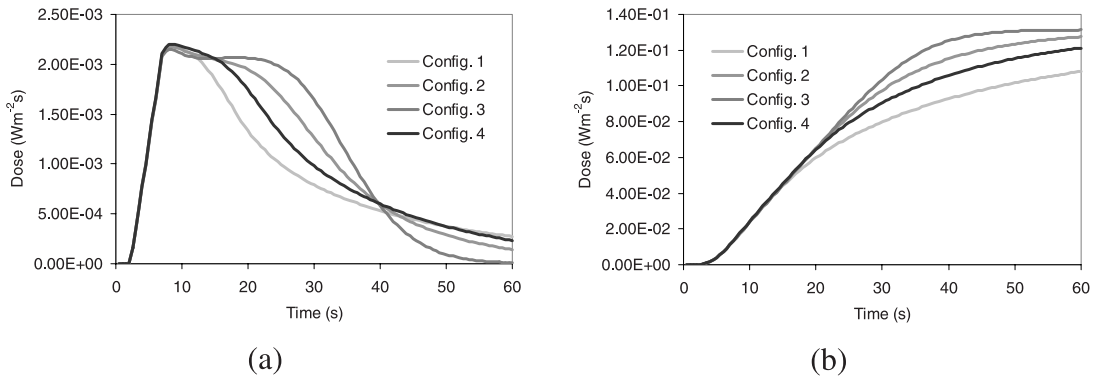

Figure 14 | Variation of dose at the outflow with time: (a) instantaneous value; (b) cumulative total.

CONCLUSIONS

It is clear from the results of this study that there is significant variation in the dosages received by water as it passes through the different configurations. Using the two criteria of minimal pressure drop and most efficient exposure, configuration 3 is seen to be the best geometry. By minimising the offset of the inlet and outlet pipes from the ends of the main tube, it is possible to cut out areas of almost stagnant flow. Configuration 4 is used most widely in the industry but could be modified without too much extra engineering, to the more efficient design of configuration 3.

Specific points to come out of the CFD modelling are:

- The Reynolds Stress Model gives different predictions of turbulent kinetic energy, but similar predictions of velocities and dosage.
- Higher-order differencing for momentum is necessary for accurate solutions.
- Grid independence can be achieved with relatively low numbers of cells.

More generally, it can be seen that the CFD approach is useful in evaluating different designs for UV treatment plants. It gives a fast and efficient process for comparing designs. The use of an unstructured mesh was valuable in reducing development time. The ability to analyse through design factors, such as dosage and attenuation of a plug dose, added to the usual CFD results for velocity and pressure. These results demonstrate a technical basis for an internet-based system for design that would allow small-scale users to access the benefits of CFD in a distributed environment. This is the next stage of this project. Additional future work will be carried out to include absorption, different designs and varying particle sizes.

REFERENCES

AEA Technology 1999*a* *CFX5.3 User Guide, 8.19*, Harwell, Didcot, UK.

AEA Technology 1999*b* *CFX User Conference, Friedrichshafen, Germany*. Published on CD-ROM by CFX International.

Cairns, W. L. & MacDonald, A. A. 1995 Advances in UV disinfection technology for treatment of low quality wastewater, *Australian Water & Wastewater Association 16th Federal Convention, Sydney, Australia, April*.

van Doormaal, J. 1999 *CFX-ProMixus–CFD for mixing in the process industries*. CFX Update No. 18, Autumn.

Falconer, R. A. 1992 *Proceedings of the Second International Conference on Hydraulic and Environmental Modelling of Coastal, Estuarine and River Waters*. Gower Technical, Aldershot, UK.

Hutchinson, B. R. & Raithby, G. D. 1986 A multigrid method based on the additive correction strategy. *Numer. Heat Transfer* **9**, 511–537.

Launder, B. E., Reece, G. J. & Rodi, W. 1975 Progress in the development of a Reynolds Stress turbulence model. *J. Fluid Mech.* **68** (3), 537–566.

Launder, B. E. & Spalding, D. B. 1974 The numerical computation of turbulent flows. *Comput. Meth. Appl. Mech. Engng* **3**, 269–289.

Morvan, H. P., Pender, G., Wright, N. G. and Ervine, D. A. 2000 Three-dimensional hydrodynamics of meandering compound channels. *ASCE J. Hydraul. Engng* July, to be published.

Raw, M. J. 1994 A coupled algebraic multigrid method for the 3D Navier–Stokes equations. *10th GAMM Seminar, Kiel*.

Rhie, C. M. & Chow, W. L. 1982 *A numerical study of the turbulent flow past an isolated airfoil with trailing edge separation*. AIAA Paper 82-0998, 1982.

Richards, K. A., Wright, N. G., Baker, C. J. & Baxendale, A. 2000 Computational modelling of pollution dispersion in the near wake of a vehicle. *Proceedings of the MIRA International Conference on Aerodynamics, October*.

Schneider, G. E. & Raw, M. J. 1987 Control-volume finite element method for heat transfer and fluid flow using co-located variables–1 Computational procedure. Numer. *Heat Transfer* **11**, 363–390.

Straw, M. P. 2000 Computation and measurement of wind induced ventilation. *PhD thesis*, University of Nottingham.

Versteeg, H. K. & Malalasekera, W. 1996 *An Introduction to Computational Fluid Dynamics–The Finite Volume Method*, Longman Scientific, London.

Wright, N. G. & Easom, G. J. 1999 Comparison of several computational turbulence models with full-scale measurements of flow around a building. *J. Wind Struct.* **2**(4), 305–323.

Yakhot, V., Orsag, S. A., Thamgam, S., Gatski, T. B. & Speziale, C. G. 1992 Development of turbulence models for shear flows by a double expansion technique. *Phys. Fluids* A **4**, 1510–1520.